



# PCCP

## Structural correlations tailor conductive properties in polymerized ionic liquids

Journal:	<i>Physical Chemistry Chemical Physics</i>
Manuscript ID	CP-ART-04-2019-002268.R2
Article Type:	Paper
Date Submitted by the Author:	05-Jun-2019
Complete List of Authors:	<p>Doughty, Benjamin; Oak Ridge National Laboratory, Chemical Sciences Division            Genix, Anne-Caroline; Laboratoire Charles Coulomb            Popov, Ivan; Oak Ridge National Laboratory,            Li, Bengrui; University of Tennessee Knoxville, Department of Chemistry            Zhao, Sheng; University of Tennessee Knoxville, Department of Chemistry            Saito, Tomonori; Oak Ridge National Laboratory, Chemical Sciences Division            Lutterman, Daniel; Oak Ridge National Laboratory            Sacci, Robert; Oak Ridge National Laboratory            Sumpter, Bobby; Oak Ridge National Laboratory, Center for Nanophase Materials Sciences; Oak Ridge National Laboratory, Center for Nanophase Materials Sciences            Wojnarowska, Zaneta; University of Silesia in Katowice Institute of Physics, Institute of Physics; Oak Ridge National Laboratory, Chemical Sciences            Bocharova, Vera; Oak Ridge National Laboratory, Chemical Sciences</p>

SCHOLARONE™  
Manuscripts

# Structural correlations tailor conductive properties in polymerized ionic liquids

Benjamin Doughty<sup>1\*</sup>, Anne-Caroline Genix<sup>2\*</sup>, Ivan Popov<sup>1</sup>, Bingrui Li<sup>3</sup>, Sheng Zhao<sup>3</sup>, Tomonori Saito<sup>1</sup>, Daniel A. Lutterman<sup>1</sup>, Robert L. Sacchi<sup>1</sup>, Bobby G. Sumpter<sup>4,5</sup>, Zaneta Wojnarowska<sup>1,6</sup>, Vera Bocharova<sup>1\*</sup>

## AUTHOR ADDRESS:

1. Chemical Sciences Division, Oak Ridge National Laboratory, Oak Ridge, TN 37831, USA
2. Laboratoire Charles Coulomb (L2C), Université de Montpellier, CNRS, F-34095 Montpellier, France
3. Department of Chemistry, University of Tennessee, Knoxville, Tennessee 37996, United States
4. Center for Nanophase Materials Sciences, Oak Ridge National Laboratory, Oak Ridge, Tennessee 37831, US
5. Computational Sciences & Engineering Division, Oak Ridge National Laboratory, Oak Ridge, Tennessee 37831, USA
6. Institute of Physics, University of Silesia, SMCEBI, 75 Pulku Piechoty 1A, 41-500 Chorzow, Poland

Notice: This manuscript has been authored by UT-Battelle, LLC under Contract No. DE-AC05-00OR22725 with the U.S. Department of Energy. The United States Government retains and the publisher, by accepting the article for publication, acknowledges that the United States Government retains a non-exclusive, paid-up, irrevocable, world-wide license to publish or reproduce the published form of this manuscript, or allow others to do so, for United States Government purposes. The Department of Energy will provide public access to these results of federally sponsored research in accordance with the DOE Public Access Plan (<http://energy.gov/downloads/doe-public-access-plan>).

**ABSTRACT** Polymerized ionic liquids (PolyILs) are promising materials for applications in electrochemical devices spanning from fuel cells to capacitors and batteries. In principle, PolyILs have a competitive advantage over traditional electrolytes in being single ion conductors and thus enabling a transference number close to unity. Despite this perceived advantage, surprisingly low room temperature ionic conductivities measured in the lab raise an important fundamental question: how does the molecular structure mediate conductivity? In this work, wide-angle X-ray scattering (WAXS), vibrational sum frequency generation (vSFG), and density functional theory (DFT) calculations were used to study the bulk and interfacial structure of PolyILs, while broad band dielectric spectroscopy (BDS) was used to probe corresponding dynamics and conductive properties for a series of the PolyIL samples with tunable chemistries and structures. Our results reveal that the size of the mobile anions has a tremendous impact on chain packing in PolyILs that wasn't addressed previously. Bigger mobile ions tend to create a well-packed structure, while smaller ions frustrate chain packing. The magnitude of these changes and level of structural heterogeneity are shown to depend on the chemical functionality and flexibility of studied PolyILs. Furthermore, these experimental and computational results provide new insight into the correlation between conductivity and structure in PolyILs, suggesting that structural heterogeneity helps to reduce the activation energy for ionic conductivity in the glassy state.

## INTRODUCTION

Polymerized ionic liquids (PolyILs) represent a relatively new class of materials that combine the high charge density of ionic liquids (ILs) with the superior and tunable mechanical properties of polymers.<sup>1-6</sup> Such a commingling of properties makes PolyILs attractive candidates for applications,<sup>7-10</sup> for instance, as electrolytes in electrochemical devices. PolyILs are single ion conductors because the ions attached to the polymer chains do not contribute to the ionic conductivity. This allows the transference number for the mobile ion to approach one, providing significant advantages over traditional polymer electrolytes for applications in batteries.<sup>8, 9, 11</sup> Despite these perceived advantages, PolyILs suffer from relatively low ionic conductivity at ambient temperature, which impedes their widespread use. As a consequence, developing a molecular level understanding of the structure of PolyILs and establishing a link between the structure and conductivity are clearly necessary for the rational design of new PolyILs with improved performance.

To date, an evolving physical description of the PolyIL bulk structure has been obtained from a series of simulations<sup>12, 13</sup> and experiments.<sup>14-16</sup> From these results, it is believed that PolyILs, similar to ILs<sup>17-22</sup> and ionomers,<sup>23, 24</sup> assume structures spanning multiple length scales originating from interactions of ionic, polar and non-polar moieties. This is evidenced by X-ray scattering<sup>14, 15</sup> measurements showing multiple scattering peaks, indicative of characteristic length scales within the polymer. From MD simulation<sup>12-13</sup> the origin of the low- $q$  peak in PolyILs has been linked to polar-apolar alternation where its position appears to correlate with the backbone-to-backbone distance. The peak in the low- $q$  range ( $q \approx 0.4-0.7 \text{ \AA}^{-1}$ ), corresponding to the nanometer spatial scale, represents a signature of mesoscopic organization in PolyILs that is also found in their molecular counterparts.<sup>19, 20, 25-31</sup> The influence of various structural factors on backbone-to-backbone distance has been studied in alkyl-based imidazolium PolyILs.<sup>14, 15</sup> The analysis of the length of alkyl tails shows a linear scaling with the backbone-to-backbone distance<sup>14, 15</sup> suggesting an amphiphilic (non-ionic) character of this arrangement. However, little to no effect on backbone-to-backbone distance was found in PolyILs with varying anions,<sup>14, 15</sup> which is in agreement with reports on ILs where cations,<sup>32-34</sup> due to their complex structures, were shown to be more impactful on the structure as compared to simpler anions.

Ionic materials are known to be structurally<sup>13, 14, 22, 24, 26, 35-38</sup> and dynamically heterogeneous.<sup>39-43</sup> The position and width of low- $q$  feature define what is commonly referred as structural heterogeneity that, based on various MD simulations,<sup>12, 30, 44-47</sup> can be associated with periodicity and distribution of polar and non-polar domains formed as a result of a nanophase separation. Dynamic heterogeneity has been invoked to explain anomalous solute self-diffusion in ionic materials<sup>48, 49</sup> which is responsible for the decoupling of ion transport from segmental relaxation reported in various polymers<sup>50, 51</sup> and PolyILs.<sup>52, 53</sup> There is an ongoing debate as to whether structural heterogeneity is connected with dynamic heterogeneity and anomalous transport in ionic materials. In ILs, some light has been shed on the possible connection between anomalous diffusion and structural heterogeneity.<sup>49, 54</sup> In PolyILs, it was shown that conductivity at the glass transition temperature ( $T_g$ ) might be linked to the square of the backbone-to-backbone distance.<sup>14</sup> In other literature on PolyILs, ion-to-ion correlation distances were found to be more influential on the ion conductivity.<sup>15</sup>

While more research is on the way to provide insights into structure–dynamic correlation in ionic materials it seems that the heterogeneous nature of ILs is commonly discussed through analysis of the *position* of the low- $q$  peak where the *width* of the peak is typically overlooked. Only a few papers have been reported with analysis of the width of the low- $q$  peak in ILs<sup>19, 32, 55-57</sup> where, for example, correlation between anions, peak width, and entropy of fusion have been reported.<sup>55</sup> Analyzing only the peak positions overlooks much of this key information. Furthermore, to the best of our knowledge, the width of the low- $q$  peak and its connection to ionic conductivity have not been discussed for PolyILs. In general, an important link between heterogeneity detectable through the broadening of X-ray peak and ionic conductivity has been observed in solid ceramic electrolytes, where heterogeneity tuned for example, by ball-milling<sup>58, 59</sup> was shown to improve ionic conductivity.<sup>11</sup> It is proposed that the structural disorder in these systems aids reducing the energy barrier for ion conductivity through generation of excessive free volume. Among various geometric frustration induced disorder,<sup>60</sup> excessive free volume was shown to have the strongest correlation with the increase of conductivity in superionic ceramics.<sup>61</sup>

In this study, wide angle X-ray scattering (WAXS), vibrational sum frequency generation (vSFG) spectroscopy, and broad band dielectric spectroscopy (BDS) are used in conjunction with density functional theory (DFT) calculations to study the role of the mobile ion (anions) size and pendant groups chemistry on structural organization and conductivity in imidazolium- based PolyILs. We

demonstrate that the size of mobile anion changes the backbone- to- backbone distance and significantly affects chain packing. Through analysis of width of low- $q$  peak (referred to here as the heterogeneity length in real space), indications of side chain bending have been obtained, which are supported by vSFG measurements measuring tail and backbone structures. Furthermore, analysis of the normalized heterogeneity length highlights its possible influence on the activation energy for ionic conductivity below  $T_g$ . The observed correlation suggests new ways to tune conductivity through structural adjustments.

## RESULTS AND DISCUSSION

The structures of the PolyILs studied herein are presented in Table 1. Our PolyILs can be differentiated by the structure of the pendant groups and the counterion size, which include bromine anion ( $\text{Br}^-$ ) with  $R = 0.18 \text{ nm}$ <sup>62</sup> and bis(trifluoromethane)sulfonimide (TFSI<sup>-</sup>) anions with  $R = 0.3 \text{ nm}$ <sup>63</sup>. Throughout this report, we define tails as a part of the side/pendant group starting from the end of imidazolium ring (L1 in Table 1). In our case, these are alkyl tails with  $n = 2$  (A1 and A2) and  $n = 6$  (B1 and B2), and tail of ethylene oxide oligomer (or ether) (C1 and C2). Figure 1a presents WAXS spectra from PolyILs, where we typically observe three characteristic peaks. The peaks in the scattering signal vs.  $q$ , represents contributions from different physical correlations. However, from experiments<sup>14, 15</sup> and simulations<sup>12, 13</sup> the *dominant* contributions to discrete peaks can be attributed to various well-defined intra- and close-range intermolecular correlations. For instance, the low- $q$  peak found in all polymers can be assigned to a backbone-to-backbone distance ( $q_{\text{backbone}}$ ), whereas the intermediate- $q$  peak is dominated by anion-anion correlations ( $q_{\text{anion}}$ ) and often referred to as the ‘charge peak’. Notably, the absence of charge peaks has been reported in the literature for ILs and was explained by an interference phenomenon, where peaks from cations and anions have the same periodicity but are shifted in phase.<sup>54</sup> Unfortunately, these charge peak features were not resolved/detected in the B1 and C1 polymer samples. The peak at high- $q$  describes the pendant-to-pendant group correlations. To extract the positions and the full width at half-maximum (FWHM) for all the peaks, the spectra were fit to three Lorentzian functions using the following equation:  $I(q) = I_1 S_{\text{lorenz1}} + I_2 S_{\text{lorenz2}} + I_3 S_{\text{lorenz3}} + I_c$ , where  $I_c$  is a background and  $I_{1,2,3}$  is an amplitude of each contribution to the scattered intensity. In the Bragg approximation, the repeating distance in real space is given by  $d_{\text{backbone}} = 2\pi/q_{\text{backbone}}$ , and its value

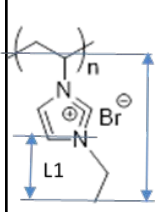
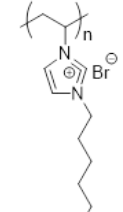
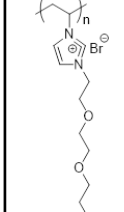
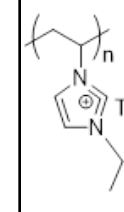
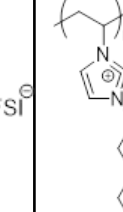
is presented in Table 1, while  $d_{\text{anion}}$  and  $d_{\text{pendant}}$  are presented in the SI. The results from fitting this function to the WAXS spectra obtained from PolyIL A1 is given in Figure S1.

Figure 1b plots these characteristic distances as a function of the length of the polymer tails in the all trans conformation. The length of the stretched tails (denoted as  $L_1$  in Table 1), as well as the total length of pendant group (denoted as  $L$  in Table 1), were estimated from DFT calculations (see details in the methods section and SI), and their values are presented in Table 1. We note that the DFT optimized PolyIL structures were in the presence of the counterions and that chain flexibility was accounted for by the calculations (room temperature ab initio MD simulations over 10 ns with the initial 3 ns used for equilibration; we note that the average RMSD for carbon was  $\sim 0.9$  Angstroms and the average end-to-end distance along the tails varied by less than 0.5 Angstroms following the equilibration stage). The lengths of the tails reported are for the monomer models and are calculated in the projection perpendicular to the backbone. The pendant-to-pendant group distances (Fig. 1b) do not vary with increasing tail length and/or changing the anion size, in agreement with literature.<sup>14, 15</sup> Notably, the anion- to-anion distance shows a non-monotonic dependence with the tail length; however, a detailed analysis is prohibited by an inability to detect/resolve those peaks in the B1 and C1 PolyILs.

In contrast to other reports for imidazolium-based PolyILs,<sup>14, 15</sup>  $d_{\text{backbone}}$  in our case does not scale with the length of the tail and anion size (Fig. 1b). Here, with the exception of A1 (the shortest tail), the Br<sup>-</sup> containing PolyILs always have larger backbone- to- backbone distances as compared to the same PolyILs with the larger TFSI<sup>-</sup> anion. To compare our result with literature, we determined the rate of increase of  $d_{\text{backbone}}$  per CH<sub>2</sub> group for alkyl based PolyILs. For A1-B1 pair this value corresponds to 0.26 nm/CH<sub>2</sub> which is larger than any value reported for imidazolium-based PolyILs. A similar rate of 0.196 nm/CH<sub>2</sub> has been reported from analysis of the position of the low- $q$  peak for ILs<sup>19, 56</sup> where it was concluded that tails do not overlap. Changing the counterion in the PolyIL sample leads to a significantly lower rate of 0.08 nm/CH<sub>2</sub>, as measured for the A2-B2 pair. This value agrees with 0.1 nm/CH<sub>2</sub> obtained from simulations of identical structures reported in.<sup>12, 13</sup>

**Table 1:** Structure and properties of PolyILs studied herein;  $d_{\text{backbone}}$ - backbone-to-backbone distance obtained from WAXS measurements;  $\xi_{\text{backbone}}/d_{\text{backbone}}$  is the normalized value for

heterogeneity length calculated from the width and position of low-  $q$  peak from X-ray;  $d_{\text{backbone stretched}}$  is calculated from DFT as two lengths of the side group ( $L$ ) in the all trans conformation, the detailed optimized geometries of studied molecules obtained from DFT are present in SI; The length of the stretched tails ( $L1$ ) is calculated from DFT;  $E_a$  is an activation energy of conductivity at  $T < T_g$  obtained from BDS data (Fig S5);  $T_g$  is estimated from SC curves reported in Fig S6.

	A1	B1	C1	A2	B2	C2
						
$d_{\text{backbone}}$ , nm (WAXS)	1.082 $\pm 0.02$ 1	2.121 $\pm 0.01$ 1	1.884 $\pm 0.01$ 2	1.470 $\pm 0.03$ 2	1.802 $\pm 0.01$ 1	1.558 $\pm 0.01$ 1
$\xi_{\text{backbone}}/d_{\text{backbone}}$	1.37 $\pm 0.23$	3.44 $\pm 0.21$	1.90 $\pm 0.23$	1.37 $\pm 0.23$	2.80 $\pm 0.25$	4.89 $\pm 0.30$
$d_{\text{backbone stretched}}$ ( $2 * L$ ), nm (DFT)	1.22	2.10	2.92	1.14	2.08	2.90

Length of stretched tail (L1), nm (DFT)	0.25	0.77	1.20	0.25	0.76	1.19
$T_g$ , °C	239	206	81	56	20	-12
$E_a$ below $T_g$ , kJ/mol	$80 \pm 1$ 0	$97 \pm 1$ 0	$90 \pm 1$ 0	110 $\pm 10$	$123 \pm 1$ 0	$130 \pm 1$ 0

The longest tail PolyILs with an ethylene oxide clearly exhibit a smaller increase in  $d_{backbone}$  as compared to the alkyl tail containing PolyILs (dashed lines in Fig 1B). This result indicates that the chemical structure of the tail also plays a key role and can dramatically affect the overall chain packing in the material. This is especially pronounced in the case of C2, which shows only slight increase in the backbone-to-backbone distance in respect to A2 with the shortest tail.

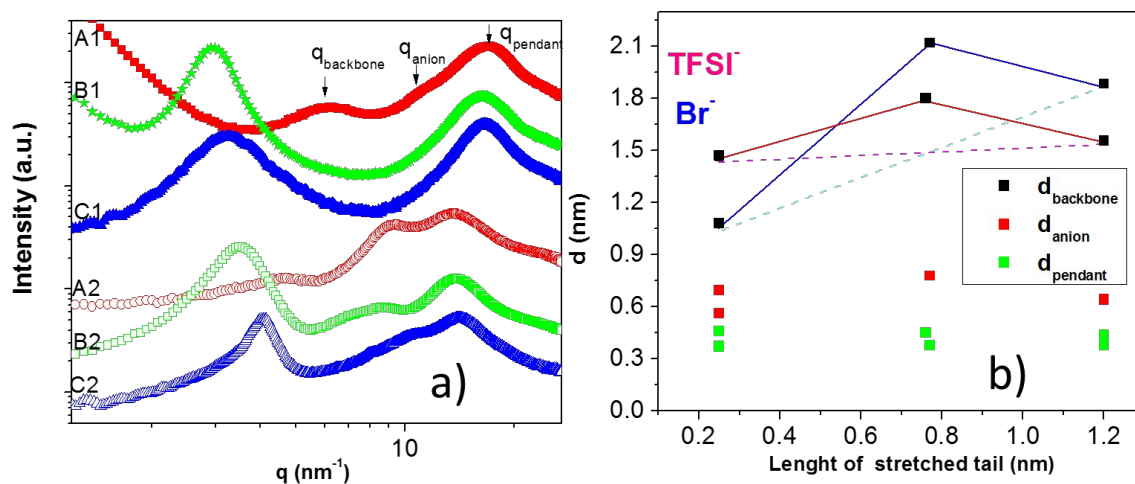


**Figure 1:** a) Wide angle X-ray scattering spectra of PolyILs presented for two different counterions: Br anion (A1, B1, C1) and TFSI anion (A2, B2, C2). Spectra were arranged to reflect increase in the length of

*the pendant group where the A-type of polymer has the shortest and the C-type the longest. For clarity, the X-ray data are vertically shifted. b) Backbone-to-backbone ( $d_{backbone}$ ), anion-anion ( $d_{anion}$ ), and pendant-to-pendant groups ( $d_{pendant}$ ) distances obtained from  $d=2\pi/q$  as a function of the length of stretched tails obtained from DFT calculations. Error bars are on the order of the symbols. The dashed lines are drawn as a guidance for the eye. In the sample name index '1' is referred to Br anion while '2' is to TFSI.*

Partial or complete pendant group interdigitation has been suggested as one possible reason leading to a decrease in the periodicity length in ILs,<sup>33, 55-56</sup> and backbone-to-backbone distance in PolyILs.<sup>14-16</sup> To estimate the degree of side group overlap in PolyILs we used the following equation

$$\text{Overlap} = 1 - d_{backbone}/(2 \cdot L) \quad (1)$$

where L is the length of the entire pendant group including the imidazolium ring in all trans conformations obtained from DFT calculations (Table 1). In this definition, a zero value corresponds to non-overlapped structures, while the value of 0.5 describes structures with fully overlapped pendant groups. Figure 2a presents the relationship between the degree of pendant group spatial overlap as estimated using Eq. (1) and the length of the stretched tail. Br<sup>-</sup> containing PolyILs with long tails (B1 and C1) have less pendant group overlap as compared to their TFSI counterparts (B2 and C2) (Fig. 2a). Furthermore, for A2 with the shortest tail, the backbone-to-backbone distance from WAXS was found to be 1.47 nm while estimates using the length of two side chain from the DFT adds to 1.14 nm (Table 1). This suggests that the backbones are separated by a distance greater than the length of two pendant group in the all trans conformation. This is in contrast with the behavior of A1 that shows some degree of tail overlap. The ethylene oxide based PolyILs are in general more overlapped comparing to the alkyl based PolyILs. This observation reveals the important role of interactions between the tail and anions, which influences the degree of phase separation in the material. Since the ethylene oxide tail can form hydrogen bonds with imidazolium cation,<sup>25, 28, 64, 65</sup> the ionic and non-ionic parts of these PolyILs are less phase separated in contrast to the behavior of alkyl based PolyILs.

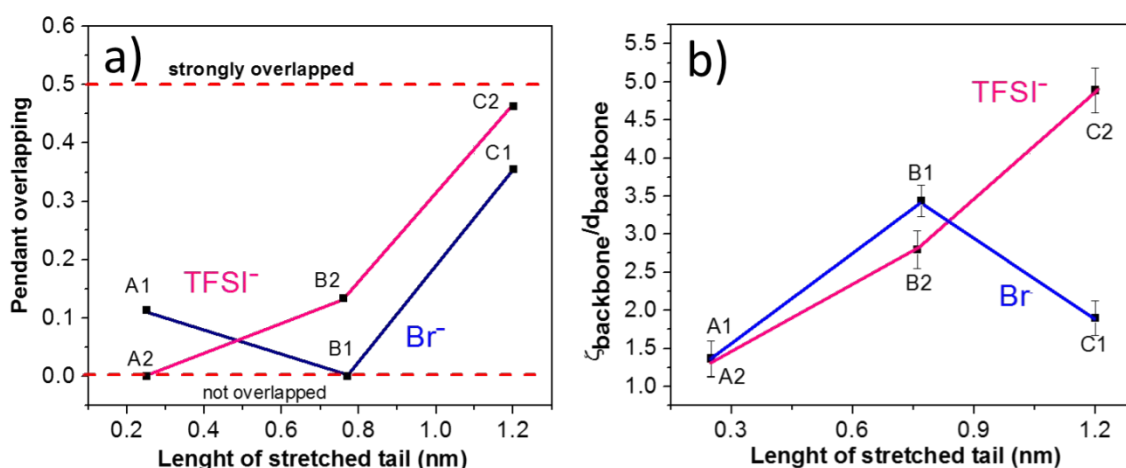


**Figure 2:** **a)** Pendant group overlap calculated using Eq. (1). The dashed lines present the limits, where zero represents no interdigitation while strong interdigitation is described as dashed line at 0.5. **b)** Normalized heterogeneity length  $\xi_{backbone}/d_{backbone}=q_{backbone}/\Delta q_{backbone}$  plotted vs length of the stretched tail calculated from DFT. Lines are only guidance for eyes.

The increase in the overlap parameter (Eq. (1)) can be caused by chain interdigitation as well as chain tilting/bending.<sup>55</sup> To separate tail bending from interdigitation a parameter that reflects the side chain packing needs to be identified. The analysis of the width of the low- $q$  peak in IL suggests that it can be used to identify tail interdigitation<sup>55</sup> as a sharper peak is a prerequisite of a long-range translation order. The FWHM ( $\Delta q_{backbone}$ ) of the low- $q$  peak is used to characterize the heterogeneous nature of IL on the mesoscale. In a real space this corresponds to the correlation<sup>55</sup> or heterogeneity length  $\xi_{backbone} = 2\pi/\Delta q_{backbone}$  responsible for fluctuations in  $d_{backbone}$ . The larger widths reflects larger local fluctuations in the distances and smaller  $\xi_{backbone}$ , indicating a less ordered structure, whereas a larger correlation length suggests a more ordered structure. A normalized heterogeneity length is represented as  $\xi_{backbone}/d_{backbone} = q_{backbone} / \Delta q_{backbone}$  and summarized for all PolyILs in Table 1 whereas values for  $\xi_{anion}/d_{anion}$  and  $\xi_{pendant}/d_{pendant}$  are presented in Table S1 in SI.

The normalized values for heterogeneity length  $\xi_{backbone}/d_{backbone}$  vs. the length of the stretched tail are plotted in Figure 2b. The most homogeneous chain packing is found for C2, while the most disordered structures are C1 and A-type of PolyILs with the shortest tails. Fig. 2b suggests that for

PolyILs containing TFSI<sup>-</sup> there is an increase in the heterogeneity length that correlates with the increase in the length of the tail. This agrees with the observation that the extent of chain overlap in these PolyILs scales approximately linearly with the length of the tail (Fig. 2a). These correlations suggest that the tails of TFSI<sup>-</sup> containing PolyILs tend to interdigitate as the tail length increases yielding more homogeneously packed structure and is in line with literature reports on imidazolium-based PolyILs with alkyl tails.<sup>12, 14, 15</sup> In contrast, there is no obvious correlation between the normalized heterogeneity length and the length of the tail for Br<sup>-</sup> containing PolyILs (Fig. 2b). For A- and B- types of the PolyILs the heterogeneity length does not change significantly with the type of the mobile ion, whereas a striking difference in  $\xi_{backbone}/d_{backbone}$  was found for C-type PolyILs. This might be indicative of different side chain packing mechanism in C1 and C2 samples.

To provide complementary insight into the ordering and packing of C1 and C2 we employed vSFG spectroscopy. It is important to emphasize that vSFG is a nonlinear optical technique that takes advantage of local symmetry. As such, it can be used to characterize ordering and packing near the interface that can be connected to the bulk given that: 1) the air-polymer interface will preferentially attract the hydrophobic backbone of the PolyILs, leaving the charged headgroups and pendant tails pointing into the bulk,<sup>66</sup> and 2) previous experimental and theoretical work suggests a similarity between the bulk and vacuum interfacial properties of ILs specifically for ether-based species.<sup>26</sup> Notably, vSFG can directly probe the conformation of the molecular species due to the sensitivity to local symmetry, which allows these measurements to provide insight into how PolyIL tails and backbones pack and order. Figure 3 shows vSFG spectra for the C1 and C2 samples probed in this work. To assist in peak assignments we used scaled frequencies obtained from normal mode DFT calculations in combination with vSFG selection rules; key bands are shown as solid/dashed lines in the spectra in Figure 3 along with their assignments from DFT.<sup>67</sup>

The prominent bands near 2827 cm<sup>-1</sup> in the vSFG spectra are readily assigned the -CH<sub>2</sub> symmetric stretch (-CH<sub>2</sub>-ss) from the long ethylene oxide tails branching off the imidazolium ring (structure in Table 1, marked in Figure 3 as the solid blue line). Notably, the strong signal from methylene groups from C1 polymers with Br<sup>-</sup> counterions is indicative of gauche conformers in the tail and an overall distorted/bent structure.<sup>68-70</sup> In contrast, the larger TFSI<sup>-</sup> anions result in tails that are generally more extended, which is realized by significant suppression of the peak near 2827 cm<sup>-1</sup>

as seen in Fig. 3a. A similar trend is found for the feature at  $\sim 2887\text{ cm}^{-1}$  in the PPP spectra that is assigned to the methylene asymmetric stretch on the tail for C1 and C2 samples. This peak is most evident in the PPP polarization combination, which supports its assignment to an asymmetric stretching mode, and is also in line with DFT calculation (again, labeled with solid blue line) that is found near  $2883\text{ cm}^{-1}$ .

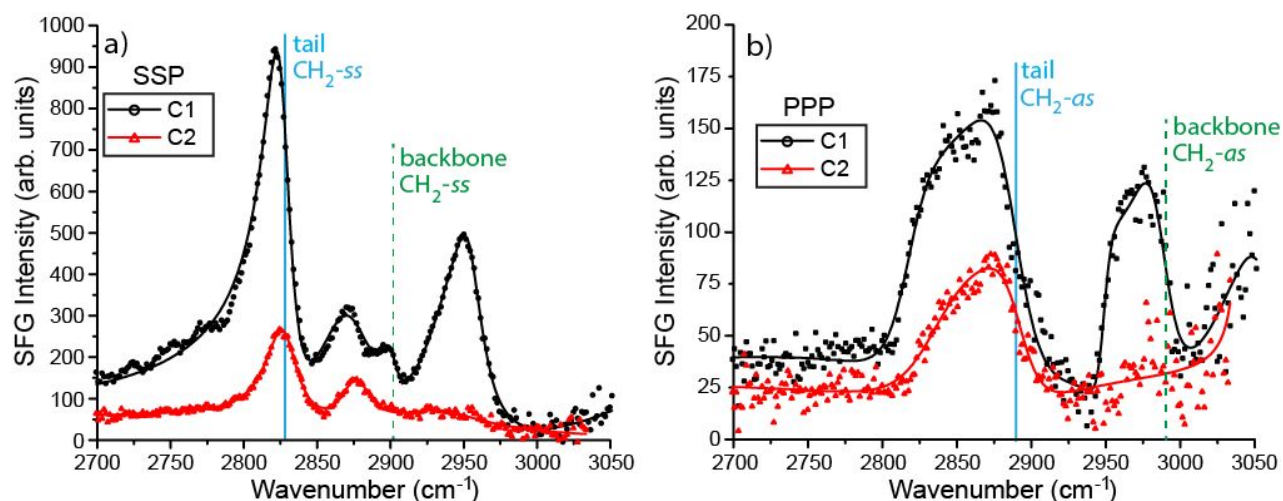


**Figure 3:** *v*SFG spectra for the C1 and C2 PolyILs studied here. Data is represented by points and the solid line is the fit to the data as described in the text. DFT calculated band positions are marked with a solid (for ethylene oxide tail) and dashed (for backbone) vertical lines and with associated labels.

The backbone disorder can be characterized through analysis of  $\text{CH}_2\text{-ss}$  stretches that are predicted by DFT calculations to be found at  $\sim 2892\text{ cm}^{-1}$  for C1 and C2 (denoted as dashed green line and label). Indeed, a feature at  $\sim 2900\text{ cm}^{-1}$  is observed in the SSP polarization combination for Br sample while absent for TFSI- sample (Fig. 3a). This indicates that the polymer backbone is more ordered for the larger anions and become more disordered as the anion size decreases. This is because the spacing of the methylene groups is such that in the limit of a perfectly ordered backbone, all the methylene groups would be pointed in the opposite direction and destructively interfere. Given that features near  $2900\text{ cm}^{-1}$  are observed in Fig. 3a for polymer C1 but not for polymer C2, it would suggest that the chains are more ordered for bigger anions, and disordered/coiled for smaller, which agrees with the analysis of heterogeneity length from the X-ray scattering measurement discussed above. This is consistent with other higher frequency modes,

such as those seen in the near the  $2980\text{ cm}^{-1}$  spectral range in the PPP spectra for C1 and C2 polymers, which correspond to methylene backbone asymmetric stretches based on our DFT calculations (marked with dashed green line with label predicted at  $\sim 2981\text{ cm}^{-1}$ ) and vSFG selection rules. Specifically, for the backbone  $-\text{CH}_2$ -*as* mode, only a modest signal is seen in the PPP spectrum for Br<sup>-</sup> containing PolyILs, whereas this feature is again lost in the TFSI<sup>-</sup> anion PolyILs. The remaining peaks and their assignments for the C1 and C2 polymer are discussed in the SI. The A-type of PolyILs are generally found to be more disordered than the C-type, but the same trend that the TFSI<sup>-</sup> orders the polymer better than Br<sup>-</sup> is preserved (data presented in SI). For A-type polymers, we observe far fewer peaks in the vSFG spectra with a much weaker overall intensity as compared to those C-type PolyILs discussed above.

Based on the cumulative results of our structural studies we arrive at an intuitive physical picture describing the chain organization in PolyILs that balances two critical factors: 1) the difference in the chemistry of the tails and 2) the size of the anions. Br<sup>-</sup> anions have a radius almost twice smaller than that of TFSI<sup>-</sup>, which implies stronger electrostatic interactions. To screen this interaction several neighboring molecules must be involved. For instance, from previous simulation work,<sup>71</sup> it was demonstrated that the hexafluorophosphate (PF<sub>6</sub><sup>-</sup>) anion, which is slightly larger than Br<sup>-</sup>, is surrounded by four positively charged neighbors. A similar situation is possible for the A1 polymer, where due to the very short pendant groups, anions can be shared by several cations of adjacent chains (Figure 4a) serving as a chain crosslinker. This obviously will lead to a drastic decrease in  $d_{\text{backbone}}$  and therefore drive a certain degree of backbone and pendant group disorder that were observed in the analysis of heterogeneity length from X-ray measurements and confirmed in vSFG studies. In A2 PolyILs side groups are not interdigitated and separated further than the length of two extended side groups (Fig. 4b). This might be explained by the presence of bulky TFSI<sup>-</sup> anions that cannot be accommodated by such a short tail. Bulky anions cause an additional steric chain repulsion, which contributes to the increase in the backbone-to-backbone distances and higher disorder observed in our experiments.

When the length of pendant group increases the effect of anion size and differences in the chemistry of the tails become more pronounced. For instance, the presence of Br<sup>-</sup> anions leads to a disruption of the tail interdigitations, yielding an overall increase in  $d_{\text{backbone}}$  compared to PolyILs containing TFSI<sup>-</sup>. The magnitude of this effect depends on the polarity and flexibility of the tails.

From the analysis of chain overlap in B1, the diminished interdigitation results in polymer chain separation by the length of stretched tails. Generally, B-type of polymers have more extended tails and overall higher values of  $d_{\text{backbone}}$  compared to C-type PolyILs. This is because non-polar alkyl tails tend to phase separation from ionic parts, which is further enhanced by the presence of Br<sup>-</sup> anions. Observation of extended alkyl tails is also in line with literature reports on ionic liquids.<sup>32, 56, 72</sup> Schematically structure of B-type of PolyILs are presented in Figs. 4c and 4d.

In the case of the C-type of PolyILs the tails can adopt multiple gauche conformations due to the extreme flexibility of the ether linkage. The degree of tail curling depends on the anion size where for smaller anions (Br<sup>-</sup>), the tails and polymer backbone are found to be more bent/distorted whereas for larger anions (e.g., TFSI<sup>-</sup>) the tails are generally more extended. From the literature on IL, it is known that ether tails tend to curl toward the cation head<sup>25, 28, 64, 65</sup> effectively reducing electrostatic interaction. Based on analysis of heterogeneity length and results of vSFG we believe that in case of C1 tails are bent to the cation on the same chain, which will disrupt tail packing thereby increasing disorder, while in C2 the tails tend to reach out to cation on the adjacent chain to enhance tail overlap and reduce the number of gauche conformers. This improves packing. The postulated structures for C1 and C2 are sketched in Figs. 4e and f.

In the case of TFSI<sup>-</sup> based PolyILs we believe that reduction in the backbone-to-backbone distance and decrease in disorder are governed by differences in the degree of pendant group interdigitation: the longer tails lead to a better packing and reduced heterogeneity. In case of Br<sup>-</sup>-containing PolyILs, a change in the backbone-to-backbone distances is due to the frustration in tail packing with the associated magnitude depending on the functionalization of the tails. Although, the underlying mechanism of frustration in tail packing is not known, it is thought here that it might be related to the small size of anion that can mediate electrostatic interactions that must be screened by the rearrangement of the polymer matrix. Furthermore, we should emphasize the packing in PolyILs is different from traditional ILs. In ILs better ordering and packing<sup>73</sup> and even formation of liquid crystalline phase<sup>17, 74, 75</sup> is observed in case of small anion like Cl<sup>-</sup> and Br<sup>-</sup>, whereas TFSI<sup>-</sup> anions introduce more disorder because of their bulkiness, in PolyILs, we see a markedly different behavior. Here, we see a manifestation of this effect in the connectivity of the monomer resulting in a reduced mobility of the chains in PolyILs.

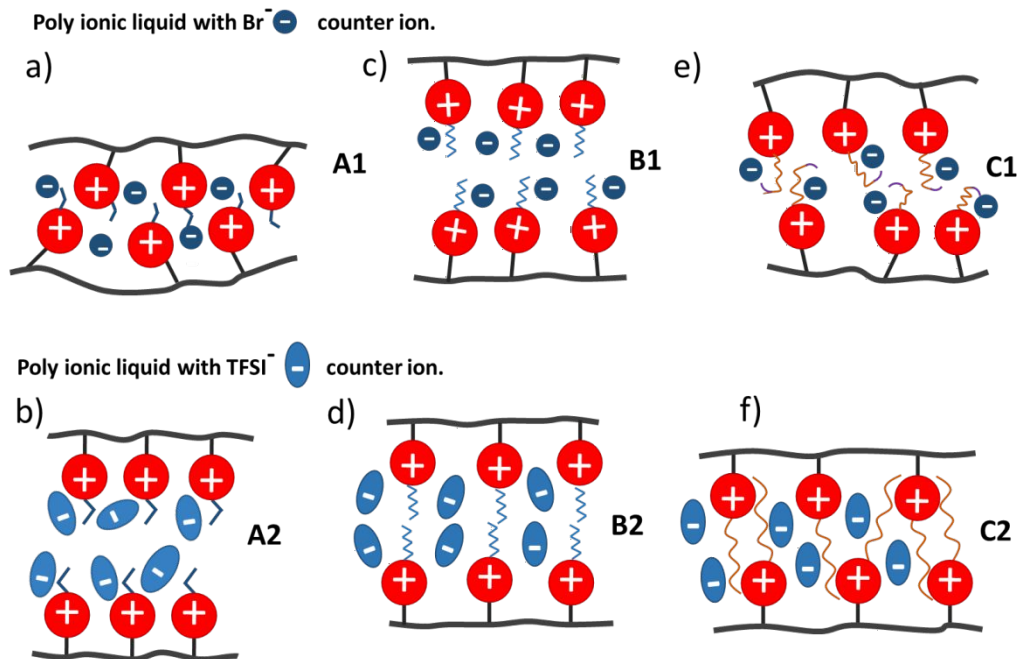


**Figure 4:** Sketches of possible structural arrangements in the PolyILs

**Correlation between conductivity and structure:** In order to establish connections between ionic conductivity and nanoscale morphology, we use the fact that the conductivity is defined as a product of the number of charge carriers and electrophoretic mobility, which is directly proportional to diffusion of the charge carriers. The diffusion in the glassy state is dominated by ion hopping which means the ion must overcome certain energy barriers to be transported from one location to another. In solid electrolytes, the heterogeneous nature of the surrounding environment is known to play an important role in lowering the energy barrier for ions to jump between various sites. Increasing probability of ion to jump leads to a decrease in activation energy ( $E_a$ ) for conductivity and advances super ionic conductivity.<sup>11, 58, 59, 61</sup> How heterogeneity is manifested in PolyIL ionic transport was, until now, not known.

To elucidate potential correlations between heterogeneity length and activation energy required for conductivity below  $T_g$ , we plot  $E_a$  vs  $\xi_{backbone}/d_{backbone}$  for all PolyILs. The activation energy for conductivity was recovered by fitting of conductivity spectra below  $T_g$  to the Arrhenius equation,  $\sigma = \sigma_0 \cdot \exp(-E_a/kT)$ . The characteristic conductivity spectra measured by BDS and example of their fitting are presented in Figure S5 in the SI. As it can be seen from Fig. 5a,  $E_a$  has a tendency to increase with increase in a value of scaled heterogeneity length (here we should

mention that the same tendency holds for heterogeneity length itself but no correlation is found for the inverse of  $d_{\text{backbone}}$ ). This tendency suggests that heterogeneous systems have lower activation barriers for ions to jump between sites which is in line with expected effect of free volume on ion diffusion. Furthermore, although three points per curve are not enough to discuss the trends, the large separation in activation energies (larger than the error bar) between PolyILs with different ions (Fig. 5a) suggest that for PolyILs with similar values of heterogeneity length the smaller mobile ions require a lower energy to make a jump. The latter is suggestive that in spite of the ionic nature, conductivity is limited by ion diffusion, which is sensitive to the rearrangement and the associated local environment but is least affected by ion pair dissociation. This observation is also in line with the earlier reported work on PolyILs,<sup>76</sup> where it was shown that activation energy can be described by two contributions: electrostatic and elastic forces. It was shown that in TFSI<sup>-</sup> containing PolyILs,  $E_a$  is dominated by the elastic force which is proportional to a macroscopic shear moduli.<sup>76</sup> In contrast, the electrostatic interaction dominates the conductivity in PolyILs with small ions like Li<sup>+</sup>, and both, elastic forces and electrostatic interactions are important for ions of intermediate size, such as Br<sup>-</sup>.

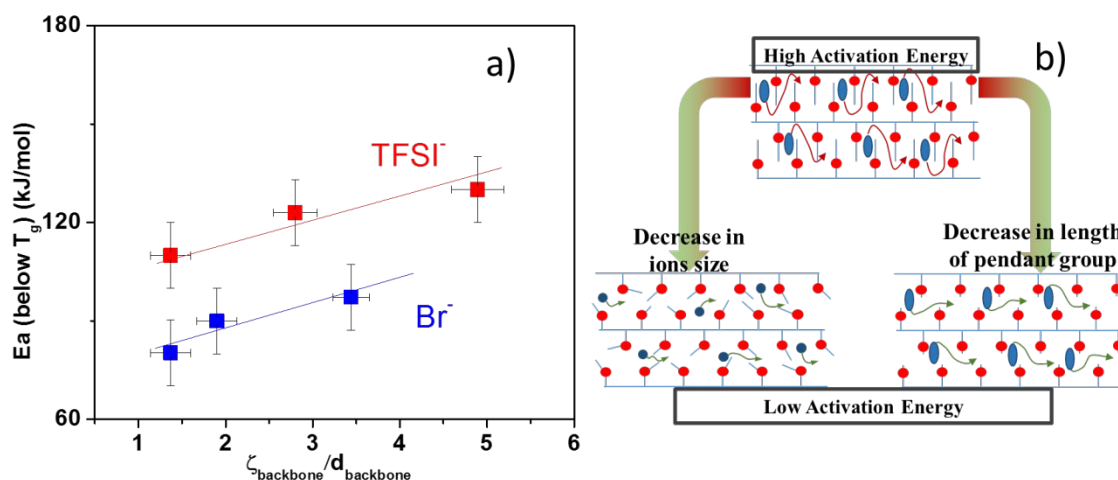


**Figure 5:** a) Activation energy for conductivity vs  $\xi_{\text{backbone}}/d_{\text{backbone}}$ ; b) Sketch illustrates that decrease in activation energy of conductivity can be achieved by frustration in chain packing through shortening the length of the tail and decrease in ion size. Lines are only guidance for eyes.

Borrowing ideas from conductive ceramics, a correlation in Figure 5a can be related to an effect of free volume that is generated due to a frustrated chain packing. A smaller heterogeneity length leads to a stronger packing disorder which generates an additional free volume. Based on our analysis, it seems that there are several structural parameters that can lead to frustration in chain packing, such as switching to a smaller anions or/and reducing the length of the side chains (see Fig. 5b). Likewise, frustration in chain packing has been pointed out as possible pathway to influence conductivity in other solid polymer electrolytes.<sup>77-79</sup> The same slope for different ions in Figure 5a suggests that the influence of the structural heterogeneity is universal, yet the different pre-factor (the offset) suggests that some other contribution is still to be accounted for. Such complex correlations is not a surprise because conductivity is a multifaceted phenomenon that is likely affected by various length and time scales and further studies are required to elucidate the exact mechanisms of those posed here.

## CONCLUSIONS

We demonstrated that the size of the anion, chemistry and length of tails affect structural organization in imidazolium-based PolyILs. Based on experimental evidence we conclude that presence of the smaller Br<sup>-</sup> anion leads to the frustration of the pendant group packing and increase in backbone-to- backbone distance comparing to corresponding TFSI<sup>-</sup> based PolyILs where tails tend to interdigitate. The magnitude of packing frustration depends on the chemistry and length of the tail. Bending of the polymer tails in the presence of Br<sup>-</sup> is detected for the very flexible tails by means of vSFG. Analysis of width of the low- $q$  peak (heterogeneity length) provides a measure to distinguish between PolyILs with interdigitated side chains and those where altering in  $d_{backbone}$  appeared as a result of frustrated packing. The validity of this approach is supported by vSFG measurements where chain conformations are directly probed. Our studies demonstrate that heterogeneity (disorder) influences activation energy for conductivity below  $T_g$ . The more heterogeneous the structure is, the lower is the energy barrier for ions transport. Overall, the shorter tails and smaller ions cause more disorder and lower activation barrier. This work points to structural and chemical knobs that can be tailored in continued work to improve PolyILs function and associated ionic transport.

## MATERIALS AND METHODS

**Synthesis.** All the PolyILs were synthesized using a similar procedure. Briefly, poly(N-vinyl imidazole) was synthesized via a conventional free radical polymerization of N-vinyl imidazole with Azobisisobutyronitrile (AIBN) and was used as the precursor for all the PolyILs. Nucleophilic substitution with 1-bromo derivatives, followed by ion-exchange and rigorous purification yields the PolyILs that differ by the structure of the pendant groups and the counterion size. The synthesis of A1, A2, C1, and C2 was reported in detail in reference <sup>80</sup>. To synthesize B1 and B2, we used 1-bromohexane (Sigma) to react with poly(N-vinyl imidazole), followed by exchanging with TFSI<sup>-</sup> following protocol in reference <sup>80</sup>.

**Wide Angle X-Ray Scattering (WAXS)** measurements were conducted using a SAXSLab Ganesha at the Shared Materials Instrumentation Facility (SMIF), Duke University, North Carolina. A Xenocs GeniX3D microfocus source was employed with a copper target leading to a monochromatic beam with wavelength  $\lambda = 1.54 \text{ \AA}$ . Calibration of the scattering vector,  $q = 4\pi \sin\theta/\lambda$ , was performed using the first order peak of silver behenate ( $q = 0.1076 \text{ \AA}^{-1}$ ). We worked with a sample-to-detector distance  $D = 1 \text{ m}$  giving a  $q$  range from 0.07 to  $2.8 \text{ \AA}^{-1}$ . The spectra are presented in Fig. 1 and detailed summary is presented in Table 1 and in the Supporting Information (SI). All measurements were done at room temperature.

**Vibrational sum frequency generation (vSFG)** is a nonlinear optical spectroscopy<sup>67, 81, 82</sup> uniquely capable of extracting interfacial molecular scale information such as ordering, chemical speciation, and orientation.<sup>70, 83-89</sup> The radiated vSFG intensity is proportional to the absolute square of the second order nonlinear susceptibility,  $\chi_{eff}^{(2)}$ , and the driving laser fields, ( $E_{IR}$  and  $E_{NIR}$ ):

$$I_{SFG} \propto |\chi_{eff}^{(2)} E_{IR} E_{NIR}|^2 \quad (2)$$

where the effective second order nonlinear susceptibility, is the sum of resonant,  $\chi_{res}^{(2)}$ , and nonresonant  $\chi_{NR}^{(2)}$  contributions

$$\chi_{eff}^{(2)} = \chi_{NR}^{(2)} + \chi_{res}^{(2)} = \chi_{NR}^{(2)} + \sum_q \frac{A_q}{\omega_{IR} - \omega_q + i\Gamma_q} \quad (3)$$

Here  $\omega_{IR}$  is the driving mid-IR laser frequency,  $A_q$  is the amplitude associated with a given molecular vibration, which is related to the interfacial population and associated molecular ordering,  $\omega_q$  is the resonant transition frequency for a given mode, and  $\Gamma_q$  is related to the linewidth. Eq.3 shows that when frequency components in the broadband IR pulse are resonant with vibrational transitions in the interfacial molecules an enhancement in the radiated vSFG is expected, thus generating an interfacial vibrational spectrum. Due to the even-order light-matter interaction, vSFG from molecules in centrosymmetric and isotropic bulk media destructively interfere – leaving only signal originating from interfacial species that coherently add.<sup>81, 82, 90</sup> This makes vSFG a surface specific spectroscopy and one uniquely capable of probing the organization of complex polymer systems due to the sensitivity to local symmetry and ordering. Details surrounding the experimental configuration for vSFG measurements can be found in our previous reports and in the SI.<sup>70, 87, 88, 91, 92</sup> The vSFG data was fit to Eqs. (2) and (3) to extract peak positions, amplitudes and linewidths. These results and associated assignments are summarized in the SI. To aid in peak assignments, DFT calculated normal mode vibrational frequencies were uniformly scaled by a 0.9877 multiplicative factor to match average experimental frequencies for the methylene transitions in the ethylene oxide tails (symmetric and asymmetric stretches) in C1 and C2 polymer samples.

**Density Functional Theory (DFT) and Ab Initio Molecular Dynamics calculations** were used to help in understanding the effects of anion size for the series of poly(N-vinyl imidazole) cations. Models of the PolyILs included: single monomers, dimers, trimers and tetramers of both the short-chain and long-chain pendant cations described in structures A-C in Table 1, to enable understanding of connectivity and pendant length effects. The anions studied were Br<sup>-</sup> and TFSI<sup>-</sup>. Calculations were performed using the Vienna *Ab Initio* Simulation Package (VASP, 5.4.4)<sup>93-95</sup> with the projector-augmented wave (PAW) method.<sup>96, 97</sup> In these simulations, the electron-ion interactions were described using standard PAW potentials and the van der Waals interactions were accounted for using the vdW-DF2 method implemented by Langreth and Lundqvist.<sup>98</sup> The Brillouin-zone integrations were performed on a  $\Gamma$ -centered  $1 \times 1 \times 1$  k-point grid and the kinetic energy cutoff for plane waves was set to 400 eV, and the “normal” precision setting was adopted. 3D periodic boundary conditions were used with a large simulation cell to allow separation of periodic images of at least 12 Angstroms. Full optimization of the all the model structures was performed followed by a normal mode analysis, from which the frequencies and eigenvectors were

compared to experimental data. To examine the room temperature behavior of the PolyILs, we also performed ab initio molecular dynamics simulations (AIMD). AIMD was performed using VASP in a canonical NVT ensemble with the temperature of the simulations maintained by a Nose-Hoover thermostat at 25 °C. For these simulations, a single molecule of the model systems and a time step of 1 fs was used, with random initial velocities assigned to all atoms according to the Maxwell-Boltzmann distribution. AIMD simulations for the different systems were carried out for at least 10 ns and the trajectories were evaluated to analyze the motion of the ions and overall changes in the molecular structure. The optimized geometries and characteristic lengths are presented in SI.

**Broadband Dielectric Spectroscopy (BDS)** was employed to collect the dielectric spectra in the frequency range of  $10^{-1} - 10^7$  Hz using Novocontrol system, which includes an Alpha-A Impedance Analyzer and a Quattro Cryosystem temperature control unit. The samples were measured using a parallel-plate configuration with stainless steel capacitors, where the separation between the electrodes was 47 micrometers to yield a geometrical capacitance of 21 pF. The samples were placed inside the cryostat with a dry nitrogen atmosphere and equilibrated at 380 K for one hour before any measurements. The samples were equilibrated for at least 15 minutes between temperatures steps to achieve thermal stabilization within 0.2 K. The glass transition temperatures of A1 and B1 samples are close to the material degradation temperature, which limits these measurements to temperatures below  $T_g$ . The activation energy of conductivity below  $T_g$  ( $E_a$ ) (Table 1) was estimated from BDS spectra by fitting the DC conductivity below  $T_g$  to the Arrhenius equation,  $\sigma = \sigma_0 \cdot \exp(-E_a/kT)$ . The BDS spectra are presented in Figure S5 in SI. Additional technical details of the measurements with BDS can be found in SI and in.<sup>76</sup>

**Differential Scanning Calorimetry (DSC)** measurements were performed on a TA Q2000 instrument. The samples sealed in aluminum pans were initially equilibrated at 423 K for one hour. The heating and cooling cycles were performed with modulation  $\pm 1^\circ$  every 60 s, ramp 2 K/min. The glass transition temperature was estimated as the mid-point of the step in specific heat on the second heating cycle. DSC curves are presented Figure S6 in SI and data are summarized in Table 1.

## AUTHOR INFORMATION

**Corresponding Authors**

\*Vera Bocharova Email: [bocharovav@ornl.gov](mailto:bocharovav@ornl.gov), Anne-Caroline Genix Email: [anne-caroline.genix@univ-montp2.fr](mailto:anne-caroline.genix@univ-montp2.fr), Benjamin Doughty, Email: [doughtybl@ornl.gov](mailto:doughtybl@ornl.gov)

**Additional information**

Correspondence and requests for materials should be addressed to \*E-Mail: [bocharovav@ornl.gov](mailto:bocharovav@ornl.gov)

**Author Contributions**

The manuscript was written through contributions of all authors. All authors have given approval to the final version of the manuscript. V.B. and A-C.G. carried out X-ray and DSC measurements, performed data analysis and interpretation, IP, ZW, SZ carrier out BDS measurements and helped with data interpretation, B.D. carried out the vSFG measurements, data analysis and interpretation. D.A.L. and R.L.S. carried out ATR-FTIR measurements and associated analysis. BGS carried out the DFT calculations and normal mode analysis.

**Notes**

The authors declare no competing financial interest.

**ACKNOWLEDGEMENTS**

We would like to acknowledge Prof. Alexei P. Sokolov for fruitful discussion and help with manuscript preparation.

This work was supported by Laboratory Directed Research and Development program of Oak Ridge National Laboratory, managed by UT-Battelle, LLC, for the U.S. Department of Energy. IP, BGS, R.L.S. acknowledge partial financial support for the data analysis and DFT calculation

and ATR-FTIR measurements by the U.S. Department of Energy (DOE), Office of Science, Basic Energy Sciences, Materials Sciences and Engineering Division. The DFT calculations were performed at the Center for Nanophase Materials Sciences which is a US DOE Office of Science User Facility.

## REFERENCES

1. M. Armand, F. Endres, D. R. MacFarlane, H. Ohno and B. Scrosati, *Nat. Mater.*, 2009, **8**, 621.
2. H. Ohno, M. Yoshizawa and W. Ogihara, *Electrochim. Acta*, 2004, **50**, 255.
3. T. Ueki and M. Watanabe, *Macromolecules*, 2008, **41**, 3739.
4. K. Yin, Z. Zhang, L. Yang and S. I. Hirano, *J. Power Sources*, 2014, **258**, 150.
5. I. Osada, H. de Vries, B. Scrosati and S. Passerini, *Angew. Chem., Int. Ed.*, 2016, **55**, 500.
6. A. Manthiram, X. Yu and S. Wang, *Nat. Rev. Mater.*, 2017, **2**, 16103.
7. X. Chen, J. Zhao, J. Zhang, L. Qiu, D. Xu, H. Zhang, X. Han, B. Sun, G. Fu, Y. Zhang and F. Yan, *J. Mater. Chem.*, 2012, **22**, 18018.
8. Y. Wang, K. S. Chen, J. Mishler, S. C. Cho and X. C. Adroher, *Appl. Energy*, 2011, **88**, 981.
9. D. Mecerreyes, *Prog. Polym. Sci.*, 2011, **36**, 1629.
10. J. Bandomir, A. Schulz, S. Taguchi, L. Schmitt, H. Ohno, K. Sternberg, K. P. Schmitz and U. Kragl, *Macromol. Chem. Phys.*, 2014, **215**, 716.

11. J. C. Bachman, S. Muy, A. Grimaud, H.-H. Chang, N. Pour, S. F. Lux, O. Paschos, F. Maglia, S. Lupart, P. Lamp, L. Giordano and Y. Shao-Horn, *Chemical Reviews*, 2016, **116**, 140-162.
12. H. Liu and S. J. Paddison, *Macromolecules*, 2017, **50**, 2889.
13. H. Liu and S. J. Paddison, *ACS Macro Letters*, 2016, **5**, 537-543.
14. D. Salas-de la Cruz, M. D. Green, Y. S. Ye, Y. A. Elabd, T. E. Long and K. I. Winey, *J. Polym. Sci., Part B: Polym. Phys.*, 2012, **50**, 338.
15. C. Iacob, A. Matsumoto, M. Brennan, H. Liu, S. J. Paddison, O. Urakawa, T. Inoue, J. Sangoro and J. Runt, *ACS Macro Lett.*, 2017, **6**, 941.
16. M. Heres, T. Cosby, E. U. Mapesa, H. Liu, S. Berdzinski, V. Strehmel, M. Dadmun, S. J. Paddison and J. Sangoro, *Macromolecules*, 2019, **52**, 88-95.
17. A. E. Bradley, C. Hardacre, J. D. Holbrey, S. Johnston, S. E. J. McMath and M. Nieuwenhuyzen, *Chem. Mater.*, 2002, **14**, 629.
18. A. Triolo, A. Mandanici, O. Russina, V. Rodriguez-Mora, M. Cutroni, C. Hardacre, M. Nieuwenhuyzen, H. J. Bleif, L. Keller and M. A. Ramos, *J. Phys. Chem. B*, 2006, **110**, 21357.
19. A. Triolo, O. Russina, H. J. Bleif and E. Di Cola, *J. Phys. Chem. B*, 2007, **111**, 4641.
20. K. Fujii, R. Kanzaki, T. Takamuku, Y. Kameda, S. Kohara, M. Kanakubo, M. Shibayama, S. ichi Ishiguro and Y. Umebayashi, *J. Chem. Phys.*, 2011, **135**, 244502.
21. C. Hardacre, J. D. Holbrey, C. L. Mullan, T. G. A. Youngs and D. T. Bowron, *J. Chem. Phys.*, 2010, **133**, 74510.
22. O. Russina, A. Triolo, L. Gontrani and R. Caminiti, *J. Phys. Chem. Lett.*, 2012, **3**, 27.
23. U. H. Choi, Y. Ye, D. Salas de la Cruz, W. Liu, K. I. Winey, Y. A. Elabd, J. Runt and R. H. Colby, *Macromolecules*, 2014, **47**, 777.
24. L. M. Hall, M. E. Seitz, K. I. Winey, K. L. Opper, K. B. Wagener, M. J. Stevens and A. L. Frischknecht, *JACS*, 2012, **134**, 574-587.
25. J. J. Hettige, W. D. Amith, E. W. Castner and C. J. Margulis, *The Journal of Physical Chemistry B*, 2017, **121**, 174-179.
26. R. Atkin and G. G. Warr, *J. Phys. Chem. B*, 2008, **112**, 4164.
27. C. Hardacre, J. D. Holbrey, S. E. J. McMath, D. T. Bowron and A. K. Soper, *J. Chem. Phys.*, 2003, **118**, 273.
28. A. Triolo, O. Russina, R. Caminiti, H. Shirota, H. Y. Lee, C. S. Santos, N. S. Murthy and E. W. Castner, *Chem. Commun.*, 2012, **48**, 4959.
29. C. Hardacre, J. D. Holbrey, M. Nieuwenhuyzen and T. G. A. Youngs, *Acc. Chem. Res.*, 2007, **40**, 1146.
30. K. Shimizu, C. E. S. Bernardes, A. Triolo and J. N. Canongia Lopes, *Phys. Chem. Chem. Phys.*, 2013, **15**, 16256.
31. M. Macchiagodena, L. Gontrani, F. Ramondo, A. Triolo and R. Caminiti, *J. Chem. Phys.*, 2011, **134**, 114521.
32. R. Hayes, S. Imberti, G. G. Warr and R. Atkin, *J. Phys. Chem. C*, 2014, **118**, 13998.
33. K. Dong, X. Liu, H. Dong, X. Zhang and S. Zhang, *Chem. Rev.*, 2017, **117**, 6636.
34. W. Zheng, A. Mohammed, L. G. Hines, D. Xiao, O. J. Martinez, R. A. Bartsch, S. L. Simon, O. Russina, A. Triolo and E. L. Quitevis, *The Journal of Physical Chemistry B*, 2011, **115**, 6572-6584.
35. T. L. Greaves, D. F. Kennedy, S. T. Mudie and C. J. Drummond, *J. Phys. Chem. B*, 2010, **114**, 10022.

36. B. Aoun, A. Goldbach, M. A. González, S. Kohara, D. L. Price and M. Saboungi, *J. Chem. Phys.*, 2011, **134**, 104509.
37. Y. Wang and G. A. Voth, *J. Am. Chem. Soc.*, 2005, **127**, 12192.
38. A. A. H. Pádua, M. F. Costa Gomes and J. N. A. Canongia Lopes, *Acc. Chem. Res.*, 2007, **40**, 1087.
39. M. G. Del Popolo and G. A. Voth, *J. Phys. Chem. B*, 2004, **108**, 1744.
40. Z. H. Hu and C. J. Margulis, *Proc. Natl. Acad. Sci. U. S. A.*, 2006, **103**, 831.
41. J. Habasaki and K. L. Ngai, *J. Chem. Phys.*, 2008, **129**, 194501.
42. D. Kim, D. Jeong and Y. Jung, *Phys. Chem. Chem. Phys.*, 2014, **16**, 19712.
43. M. Kofu, M. Nagao, T. Ueki, Y. Kitazawa, Y. Nakamura, S. Sawamura, M. Watanabe and O. Yamamuro, *J. Phys. Chem. B*, 2013, **117**, 2773.
44. J. J. Hettige, J. C. Araque and C. J. Margulis, *J. Phys. Chem. B*, 2014, **118**, 12706.
45. A. A. Freitas, K. Shimizu and J. N. Canongia Lopes, *J. Chem. Eng. Data*, 2014, **59**, 3120.
46. M. Macchiagodena, F. Ramondo, A. Triolo, L. Gontrani and R. Caminiti, *J. Phys. Chem. B*, 2012, **116**, 13448.
47. S. Li, J. L. Bañuelos, J. Guo, L. Anovitz, G. Rother, R. W. Shaw, P. C. Hillesheim, S. Dai, G. A. Baker and P. T. Cummings, *J. Phys. Chem. Lett.*, 2012, **3**, 125.
48. A. Kaintz, G. Baker, A. Benesi and M. Maroncelli, *J. Phys. Chem. B*, 2013, **117**, 11697.
49. J. C. Araque, S. K. Yadav, M. Shadeck, M. Maroncelli and C. J. Margulis, *J. Phys. Chem. B*, 2015, **119**, 7015.
50. T. Imrie, M. D. Ingram and G. S. McHattie, *J. Phys. Chem. B*, 1999, **103**, 4132.
51. Y. Wang, F. Fan, A. L. Agapov, X. Yu, K. Hong, J. Mays and A. P. Sokolov, *Solid State Ionics*, 2014, **262**, 782.
52. J. R. Sangoro, C. Iacob, A. L. Agapov, Y. Wang, S. Berdzinski, H. Rexhausen, V. Strehmel, C. Friedrich, A. P. Sokolov and F. Kremer, *Soft Matter*, 2014, **10**, 3536.
53. Z. Wojnarowska, H. Feng, Y. Fu, S. Cheng, B. Carroll, R. Kumar, V. N. Novikov, A. M. Kisliuk, T. Saito, N. G. Kang, J. W. Mays, A. P. Sokolov and V. Bocharova, *Macromolecules*, 2017, **50**, 6710.
54. J. C. Araque, J. J. Hettige and C. J. Margulis, *J. Phys. Chem. B*, 2015, **119**, 12727.
55. H. Weiss, J. Mars, H. Li, G. Kircher, O. Ivanova, A. Feoktystov, O. Soltwedel, M. Bier and M. Mezger, *The Journal of Physical Chemistry B*, 2017, **121**, 620-629.
56. O. Russina, A. Triolo, L. Gontrani, R. Caminiti, D. Xiao, L. G. Hines, R. A. Bartsch, E. L. Quitevis, N. Plechkova and K. R. Seddon, *J. Phys.: Condens. Matter*, 2009, **21**, 424121.
57. C. Hardacre, J. D. Holbrey, C. L. Mullan, T. G. A. Youngs and D. T. Bowron, *J. Chem. Phys.*, 2010, **133**, 074510.
58. B. Ruprecht, M. Wilkening, S. Steuernagel and P. Heitjans, *Journal of Materials Chemistry*, 2008, **18**, 5412-5416.
59. B. Ruprecht, M. Wilkening, A. Feldhoff, S. Steuernagel and P. Heitjans, *Physical Chemistry Chemical Physics*, 2009, **11**, 3071-3081.
60. D. A. Keen and A. L. Goodwin, *Nature*, 2015, **521**, 303.
61. A. Düvel, P. Heitjans, P. Fedorov, G. Scholz, G. Cibir, A. V. Chadwick, D. M. Pickup, S. Ramos, L. W. L. Sayle, E. K. L. Sayle, T. X. T. Sayle and D. C. Sayle, *Journal of the American Chemical Society*, 2017, **139**, 5842-5848.
62. M. Ue, A. Murakami and S. Nakamura, *Journal of The Electrochemical Society*, 2002, **149**, A1385-A1388.

63. C. Lian, K. Liu, K. L. Van Aken, Y. Gogotsi, D. J. Wesolowski, H. L. Liu, D. E. Jiang and J. Z. Wu, *ACS Energy Letters*, 2016, **1**, 21-26.
64. G. D. Smith, O. Borodin, L. Li, H. Kim, Q. Liu, J. E. Bara, D. L. Gin and R. Nobel, *Physical Chemistry Chemical Physics*, 2008, **10**, 6301-6312.
65. S. I. Lall-Ramnarine, M. Zhao, C. Rodriguez, R. Fernandez, N. Zmich, E. D. Fernandez, S. B. Dhiman, E. W. Castner and J. F. Wishart, *Journal of The Electrochemical Society*, 2017, **164**, H5247-H5262.
66. C. Aliaga, C. S. Santos and S. Baldelli, *Physical Chemistry Chemical Physics*, 2007, **9**, 3683-3700.
67. W. H.-F., G. Wei, L. R., R. Yi and W. B.-H., *International Reviews in Physical Chemistry*, 2005, **24**, 191-256.
68. C. Weeraman, A. K. Yatawara, A. N. Bordenyuk and A. V. Benderskii, *Journal of the American Chemical Society*, 2006, **128**, 14244-14245.
69. M. T. Frederick, J. L. Achtyl, K. E. Knowles, E. A. Weiss and F. M. Geiger, *Journal of the American Chemical Society*, 2011, **133**, 7476-7481.
70. B. Doughty, P. Yin and Y.-Z. Ma, *Langmuir*, 2016, **32**, 8116-8122.
71. S. Mogurampelly, J. R. Keith and V. Ganesan, *J. Am. Chem. Soc.*, 2017, **139**, 9511.
72. K. Shimizu, C. E. S. Bernardes and J. N. Canongia Lopes, *J. Phys. Chem. B*, 2014, **118**, 567.
73. J. De Roche, C. M. Gordon, C. T. Imrie, M. D. Ingram, A. R. Kennedy, F. L. Celso and A. Triolo, *Chem. Mater.*, 2003, **15**, 3089.
74. F. Nemoto, M. Kofu and O. Yamamuro, *J. Phys. Chem. B*, 2015, **119**, 5028.
75. C. J. Bowlas, D. W. Bruce and K. R. Seddon, *Chem. Commun.*, 1996, 1625.
76. E. W. Stacy, C. P. Gainaru, M. Gobet, Z. Wojnarowska, V. Bocharova, S. G. Greenbaum and A. P. Sokolov, *Macromolecules*, 2018, **51**, 8637-8645.
77. C. M. Evans, G. E. Sanoja, B. C. Popere and R. A. Segalman, *Macromolecules*, 2016, **49**, 395-404.
78. S. Y. Kim, S. Kim and M. J. Park, *Nature Communications*, 2010, **1**, 88.
79. D. Lee, H. Y. Jung and M. J. Park, *ACS Macro Letters*, 2018, **7**, 1046-1050.
80. V. Bocharova, Z. Wojnarowska, P. F. Cao, Y. Fu, R. Kumar, B. Li, V. N. Novikov, S. Zhao, A. Kisliuk, T. Saito, J. W. Mays, B. G. Sumpter and A. P. Sokolov, *J. Phys. Chem. B*, 2017, **121**, 11511.
81. C. S. Tian and Y. R. Shen, *Surface Science Reports*, 2014, **69**, 105-131.
82. H.-F. Wang, *Progress in Surface Science*, 2016, **91**, 155-182.
83. A. N. Bordenyuk, C. Weeraman, A. Yatawara, H. D. Jayathilake, I. Stiopkin, Y. Liu and A. V. Benderskii, *The Journal of Physical Chemistry C*, 2007, **111**, 8925-8933.
84. H. D. Jayathilake, J. A. Driscoll, A. N. Bordenyuk, L. Wu, S. R. P. da Rocha, C. N. Verani and A. V. Benderskii, *Langmuir*, 2009, **25**, 6880-6886.
85. Y. Rao, M. Comstock and K. B. Eisenthal, *The Journal of Physical Chemistry B*, 2006, **110**, 1727-1732.
86. J. H. Jang, F. Lydiatt, R. Lindsay and S. Baldelli, *The Journal of Physical Chemistry A*, 2013, **117**, 6288-6302.
87. B. Doughty, S. Goverapet Srinivasan, V. S. Bryantsev, D. Lee, H. N. Lee, Y.-Z. Ma and D. A. Lutterman, *The Journal of Physical Chemistry C*, 2017, **121**, 14137-14146.
88. S. Tan, M. B. Gray, M. K. Kidder, Y. Cheng, L. L. Daemen, D. Lee, H. N. Lee, Y.-Z. Ma, B. Doughty and D. A. Lutterman, *ACS Catalysis*, 2017, **7**, 8118-8129.

89. D. N. Voylov, A. P. Holt, B. Doughty, V. Bocharova, H. M. Meyer, S. Cheng, H. Martin, M. Dadmun, A. Kisliuk and A. P. Sokolov, *ACS Macro Letters*, 2017, **6**, 68-72.
90. W. Gan, R. Lu, Y. Rao and B.-H. Wu, *International Reviews in Physical Chemistry*, 2005, **24**, 191-256.
91. A. U. Chowdhury, F. Liu, B. R. Watson, R. Ashkar, J. Katsaras, C. Patrick Collier, D. A. Lutterman, Y.-Z. Ma, T. R. Calhoun and B. Doughty, *Optics letters*, 2018, **43**, 2038-2041.
92. B. R. Watson, Y.-Z. Ma, J. F. Cahill, B. Doughty and T. R. Calhoun, *Journal of Colloid and Interface Science*, 2019, **537**, 389-395.
93. G. Kresse and J. Hafner, *Physical Review B*, 1993, **47**, 558-561.
94. G. Kresse and J. Furthmüller, *Computational Materials Science*, 1996, **6**, 15-50.
95. G. Kresse and D. Joubert, *Physical Review B*, 1999, **59**, 1758-1775.
96. D. Vanderbilt, *Physical Review B*, 1990, **41**, 7892-7895.
97. G. Kresse and J. Hafner, *Journal of Physics: Condensed Matter*, 1994, **6**, 8245.
98. K. Lee, É. D. Murray, L. Kong, B. I. Lundqvist and D. C. Langreth, *Physical Review B*, 2010, **82**, 081101.

## TOC figure

